Arabian Journal of Chemistry (2020) 13, 5564–5580

King Saud University

Arabian Journal of Chemistry

www.ksu.edu.sa
www.sciencedirect.com

ORIGINAL ARTICLE

Investigations on crystal structure of a novel 3-((4,6-dimethylpyrimidin-2-yl)amino)isobenzofuran-1(3H)-one, and related theoretical studies

Zeynep Tanrıkulu Yılmaz [a], H. Yasin Odabaşoğlu [b], Pelin Şenel [c], Veselina Adımcılar [c], Taner Erdoğan [d], Ayşe Daut Özdemir [c], Ayşegül Gölcü [c,*], Mustafa Odabaşoğlu [e,*], Orhan Büyükgüngör [f]

[a] *Pamukkale University, Faculty of Engineering, Chemical Engineering Department, Denizli, Turkey*
[b] *Hayat Kimya, R&D Department, Kocaeli, Turkey*
[c] *Istanbul Technical University, Faculty of Sciences and Letters, Department of Chemistry, Istanbul 34469, Turkey*
[d] *Kocaeli Univ, Kocaeli Vocat Sch, Dept Chem & Chem Proc Technol, Kocaeli, Turkey*
[e] *Pamukkale University, Chemistry Technology Program, Kinikli 20070, Turkey*
[f] *Ondokuz Mayis University, Department of Physics, Samsun, Turkey*

Received 15 January 2020; accepted 15 March 2020
Available online 4 April 2020

KEYWORDS

Phthalide;
Crystal structure;
DFT calculations;
DNA binding;
Molecular docking

Abstract In this report, 3-((4,6-dimethylpyrimidin-2-yl)amino)isobenzofuran-1(3*H*)-one have been synthesized via reaction between phthalaldehydic acid and 2-amino-4,6-dimethylpyrimidine in 90% yields and characterized by Infrared (IR), Nuclear Magnetic Resonance (NMR), Ultraviolet–visible (UV–Vis), X-ray single crystal diffraction techniques. The single-crystal X-ray analysis shows that the title compound crystallizes in the triclinic space group P-1 with unit-cell parameters $a = 7.9351(4)$ Å, $b = 11.1687(6)$ Å, $c = 16.1281(9)$ Å, $\alpha = 73.713(5)°$, $\beta = 80.362(5)°$, $\gamma = 72.882(4)°$ and $Z = 4$. A theoretical study with hybrid functional B3LYP 6-311G (d, p) basis set have been used in calculations. The structural and electronic properties have been detailed. The title compound was screened for its antioxidant activity by (1,1-diphenyl-2-picryl hydrazyl) free radical scavenging (DPPH), Ferric ion reducing antioxidant power (FRAP), total phenolic contents (TP) assays and its ferrous ions chelating property. Electronic absorption titration, thermal denaturation measurement and viscosity techniques were used to determine the interaction between double stranded DNA (dsDNA) and compound **1**. In three techniques, the mode of binding of compound **1** to dsDNA is minor groove. The UV–Vis measurement results allowed the calculation of the binding constant showing the binding strength of compound **1** to dsDNA

* Corresponding authors.
E-mail addresses: aysegulgolcu@itu.edu.tr (A. Gölcü), mustafaodabasoglu@gmail.com (M. Odabaşoğlu).
Peer review under responsibility of King Saud University.

Production and hosting by Elsevier

https://doi.org/10.1016/j.arabjc.2020.03.013

was calculated as $8.13 \times 10^4 \pm 0.07$ L mol^{-1}. Moreover, the molecular docking calculations have been performed to investigate the compound–DNA interactions, computationally. In molecular docking calculations, it was observed that for the title compound, the lowest energy docking pose takes place in the minor groove of DNA and in addition to minor groove binding, interactions between the compound and the consecutive base pairs of DNA which may cause a partial intercalation were also observed. Results showed that title compound – DNA complex is stabilized by several hydrogen bonds, and Pi-alkyl interactions also take part in the stabilization of the complex. Binding affinities of the lowest energy docking pose of the title compound was found to be −8.3 kcal/mol.

1. Introduction

Heterocyclic compounds, are widely available in nature and play an important role in organic chemistry (Quin and Tyrell, 2010; Arora et al., 2012). The vast majority of heterocyclic compounds are pharmacologically active (Lamberth and Dinges, 2012) and some of them are in clinical use such as: *penicillin* and *cephalosporin* used as antibiotics, *vinblastine* used as anticancer chemotherapy drug, *morphine* as most potent analgesic for chronic pain, etc. Among them, *oxygen and nitrogen containing heterocycles* constitute one of the largest and most varied group of heterocycles. The literature survey gives strong pieces of evidence regarding their potential in biomedical applications, and there is a general need for the synthesis of new heterocyclic compounds (Dua et al., 2011). To adress this issue, in continuation of our previous work (Yılmaz et al., 2020), in this report we synthesized a novel 3-substituted phthalide derivative, 3-((4,6-dimethylpyrimidin-2-yl)amino)isobenzofuran-1(3*H*)-one (**1**, Fig. 1) as an oxygen and nitrogen containing heterocycle.

Isobenzofuran-1(3*H*)-ones (also known as phthalides) (**2**) (Fig. 1) (Karmakar et al., 2014) and their derivatives carry a benzene ring fused to a γ-lactone moiety. They are one of the important heterocyclic compounds occuring widely in several genera of the family *Apiceae* (Beck and Chou, 2007; León et al., 2017) and in some microorganisms such as bacteria, fungi and limeworts (Gubiani et al., 2017; Harper at al., 2003; Strobel et al., 2002). Many of the phthalides, especially 3-substituted phthalides (Everaere et al., 2001; Zhang et al., 2010; Teixeira et al., 2013; Oliveira et al., 2015; Palillero-Cisneros et al., 2018; Prlainović et al., 2018) are a subset of phthalides which represent a wide range of important biological and medicinal properties such as: antifungal and antioxidant activities displayed by *isopestacin* (**3**) (Pahari et al., 2004; Strobel et al., 2002), selective activity against leukemia cancer cell lines by a vermistatin-type molecular inhibitor - *penisimplicissin* (**4**) (Stierle et al., 2012), antiplatelet activity from a brominated 3-substituted phthalide derivative (**5**) (Ma et al., 2012), 3-*n*-butylphthalide (NBP) (**6**) as a promising therapeutic agent for ischemic stroke (Liu et al., 2007), anti-inflammatory activity observed with ligustilide (**7**) (Du et al., 2007), antibacterial activity from herbaric acid (**8**) (Gelat et al., 2017) (Fig. 2).

Additionally, all of the biochemical events necessary for the maintenance of biological life are found in the genomes of all known organisms. It is known that for the proteins of the organism in which the genomes of mixed organisms reside, the nucleic acids (genes) are arranged in separate linear sequences. The regular replication of these genetic materials directs the growth, collection and function of cellular machinery. Research has made, the central role of DNA in biological systems, a fundamental target for the diagnosis and treatment of diseases. The sequencing of the human genome demonstrates the potential benefit of DNA binding studies in molecular life sciences, as well as in the discovery of large international initiatives that produce multiple genes. Understanding the variations in genome structure and the functional significance of this condition, as well as the interaction between various nucleic acids and different molecules, is of paramount importance to human medicine. Designed small molecules that are specifically recognizable to predetermined nucleic acid (like DNA) sequences are powerful means of interpreting the human genome and are likely to ultimately become therapeutic agents. For this reason, in parallel with our continuous studies (Beyazit et al., 2019; Şenel et al., 2020; Yılmaz et al., 2020), this work, which is a part of an important master's thesis, brought together many different disciplines and examined the interaction of novel phthalide derivative with dsDNA successfully experimentally and theoretically.

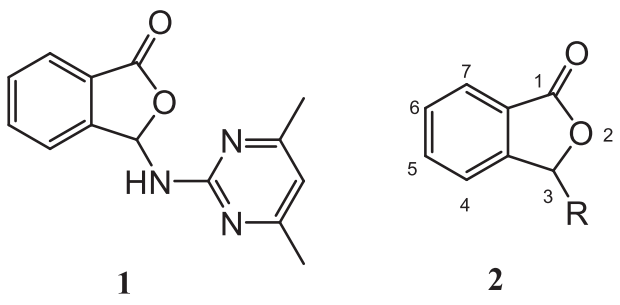

Fig. 1 3-((4,6-dimethylpyrimidin-2-yl)amino)isobenzofuran-1(3*H*)-one (**1**) and general structure of isobenzofuran-1(3*H*)-ones (**2**).

2. Experimental

2.1. Materials and chemicals

All chemicals and solvents were reagent grade and were used as purchased without any further purification. Double strain DNA (dsDNA), tris-HCl, NaCI and ethidium bromide (EtBr) were purchased from Sigma-Aldrich. All solvents were purchased from Merck. The melting point was determined by using Stuart SMP30 melting point apparatus. The Fourier Transform Infrared (FT-IR) spectra were recorded on an Agilent Cary 630 FT-IR spectrometer using solid state of compound **1**. UV–Vis absorption spectra were recorded on an OPTIZEN POP BIO UV/VIS Spectrophotometer using a 1 cm path length of the cell. The proton nuclear magnetic resonance (^{1}H NMR) measurements were recorded at an Agilent VNMRS (500 MHz) instrument. Chemical data for protons are reported in parts per million (ppm, scale) downfield from tetramethylsilane and are referenced to the residual proton in the NMR solvent (DMSO d_6: δ 2.50, or other solvents as mentioned). The chemical shifts δ are reported in parts per million (ppm), coupling constant J (expressed in Hertz). The carbon nuclear magnetic resonance (^{13}C NMR) spectra were recorded at Agilent VNMRS 126 MHz. X-Ray diffraction (XRD) data

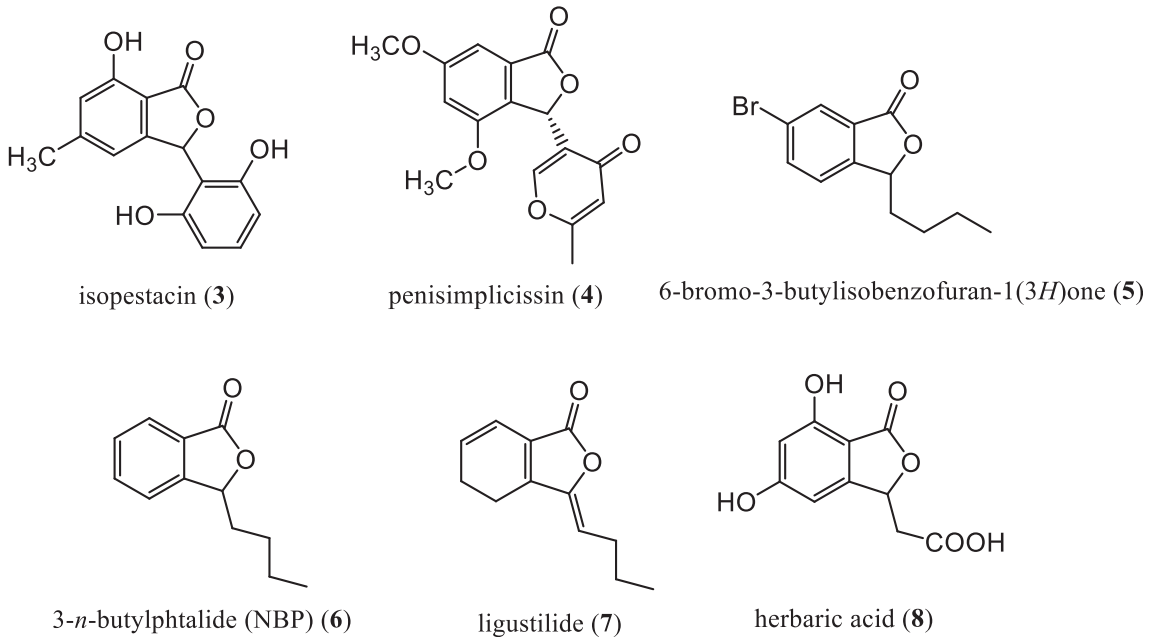

Fig. 2 3-substituted phthalides having antifungal and antioxidant (**3**), antiproliferative (**4**), antiplatelet (**5, 6**), antinociceptive and anti-inflammatory (**7**), antibacterial (**8**) activities.

was collected at 296 K with a STOE IPDS II diffractometer using MoKα radiation. The absorption spectra were recorded in the range of 200–400 nm on a T80 + UV/VIS spectrophotometer using cells of 1 cm light path and samples that contain dsDNA and compound **1** were mixed in vortex before the spectra were taken. The viscosity values of the samples were measured by using a rheometer (Haake Rheostress 1, Germany) equipped with a parallel-plate sensor (d = 35 mm, gap = 1 mm).

2.2. Synthesis of compound *1*

The compound **1** was synthesized by the reaction between phthalaldehydic acid and 2-amino-4,6-dimethylpyrimidine with 90% yield (m.p. 450.5–451 K) (Odabasoglu and Büyükgüngör, 2006). The crystals suitable for X-ray analysis were obtained by slow evaporation of the acetonitrile solution (95%) of compound **1** at room temperature. ^{1}H NMR (DMSO d_6, 500 MHz) δ 8.30 (d, J = 10.29 Hz, 1H, ArH), 7.84–7.77 (m, 2H, ArH), 7.66–7.64 (m, 2H, NH, =C—CH(O)—N), 7.45 (d, J = 10.29 Hz, 1H, ArH), 6.68 (s, 1H, ArH); 2.28 (s, 6H, CH_3). ^{13}C NMR (DMSO d_6, 126 MHz) δ 169.56, 161.17, 146.66, 134.71, 130.55, 127.76, 124.91, 124.14, 112.43, 85.01, 23.91 (Figs. S1 and S2).

2.3. Single crystal X-ray diffraction

XRD data was collected at 296 K with a STOE IPDS II diffractometer using MoKα radiation. The crystal structure was solved by direct methods using SHELXS-97. All methyl H atoms were refined using the ridding model approximation with C—H = 0.96 Å [U_{iso}(H) = 1.2U_{eq}(parent atom)]. Other hydrogen atoms were refined anisotropically by full matrix least-squares methods (Sheldrick, 1997, 2015). All H atoms were located geometrically and refined using a riding model. WinGX (Farrugia, 1999), ORTEP-3 for Windows (Farrugia, 1997) and MERCURY (Macrae et al., 2006) softwares were used for molecular drawings and other materials.

2.4. Computational details

Gaussian 09W for computational part (Frisch et al., 2010) and GaussView program for molecular visualization of calculated structures (Dennington et al., 2009) have been used. The geometry optimization was realized by crystallographically obtained geometrical data (For the geometry optimizations of two tautomers for gas phase were done at DFT level by using the hybrid functional B3LYP (Becke's three-parameter hybrid functional with LYP correlation functional) (Stephens et al., 1994) with 6-311G (d,p) basis set (Krishnan et al., 1980)). The vibrational frequencies were performed at B3LYP level and electronic excitations of the title compound by TD-DFT method, respectively (Runge and Gross, 1984; Bauernschmitt and Ahlrichs, 1996; Casida et al., 1998; Stratmann et al., 1998).

2.5. Determination of antioxidant activities

2.5.1. DPPH (1,1-diphenyl-2-picryl hydrazyl) free radical scavenging assay

1980 µL of DPPH solution (in methanol) was added to 20 µL of sample solution in DMSO with a final concentration of 20 mg/L. Samples were incubated in dark at room temperature and the absorbance was measured against the blank sample at a wavelength of 515 nm. The purple color of the solutions turn into yellow in the presence of an antioxidant molecule. The results were calculated by using radical scavenging activity (RSA) for DPPH free radical as RSA (%) = $[(A_{control} - A_{sample})/A_{control}] \times 100$ where A_{sample} is the absorbance of the sample and $A_{control}$ is the absorbance of the blank solution. Same concentration of ascorbic acid was also used as standard

substance and RSA (%) was calculated for concentration of 1 mM (Blois et al., 1958).

2.5.2. FRAP (Ferric ion reducing antioxidant power) assay

According to Benzie and Strain (1996), FRAP reagent was prepared by adding 10 mM of 2,4,6-tripyridyl-s-tri-azine (TPTZ) solution (in 40 mM HCl), 20 mM $FeCl_3 \cdot 6H_2O$ and 0.3 M acetate buffer (pH 3.6) to each other in 1:1:10 ratio respectively. 0.2 mL of sample and 1.8 mL of the FRAP reagent (warmed to the room temperature) were mixed and incubated in dark for 10 min at 37 °C. After cooling, the absorbance of the coloured product (ferrous tripyridyltriazine complex) was measured at a wavelength of 593 nm. Results were expressed as mM Fe(II)/g analyte and the calibration curve of $FeSO_4 \cdot 7H_2O$ (in distilled water) was constructed in the range of 2.5–34.0 µM with the following equation: $y = 0.031x - 0.0556$ and the regression coefficient (r^2) was 0.995.

2.5.3. Determination of TP (total phenolic) contents

0.3 mL of sample stock solution (in DMSO) was mixed with 1.5 mL of Folin-Ciocalteu's reagent (prepared via diluting 1:10 (v/v) with distilled water) and 1.2 mL of 7.5 (w/v)% aqueous sodium carbonate solution. The same procedure was performed with using 0.3 mL of DMSO as blank solution. After incubation for 15 min at room temperature, the absorbances of mixtures were measured at a wavelength of 760 nm. The results were represented as mg gallic acid equivalents (GAE) per mg of sample. The calibration equation for gallic acid (in distilled water) was $y = 0.0706x + 0.0045$ ($r^2 = 0.997$). The assay was performed also by using ascorbic acid as standard substance with the same concentration of sample solution (Singleton and Rossi, 1965).

2.5.4. Ferrous ions chelating (FIC) assay

The ferrous (Fe^{2+}) ion chelating activity of compound **1** was determined according to the method applied in some previous reports (Dinis et al., 1994, Ibrahim et al., 2013; Sellal et al., 2019). The stock solution of compound **1** was prepared in DMSO. 0.1 mL of compound **1** solution was mixed with the 0.05 mL 2 mM $FeSO_4$ and 0.2 mL of 5 mM ferrozine solution as initiator, and 0.45 mL of methanol was added. After incubation of the solutions at room temperature for 10 min, the resulting solution absorbance values were measured spectrophotometrically at a wavelength of 562 nm. Lower absorbance values of samples indicates higher ability of the molecules chelating with Fe^{2+} ions. The results were calculated as: Inhibition (%) = $[(A_{control} - A_{sample})/A_{control} \times 100]$ where $A_{control}$ is the absorbance value of the blank sample (DMSO) and A_{sample} is the absorbance of compound **1** solution.

2.6. DNA binding studies

2.6.1. Electronic absorption spectra

For DNA binding studies, 217 µM dsDNA stock solution was prepared by dilution of dsDNA to buffer solution (containing 0.2 M tris-HCI and 150 mM NaCl at pH 7.4) followed by robust stirring for two days at room temperature (kept at 4 °C for no longer than seven days). The dsDNA solution thus prepared yielded a UV absorbance ratio of 1.85 at 260 and 280 nm (A_{260}/A_{280}), indicating that dsDNA was sufficiently purified from protein contamination. In this way, the molar concentration of dsDNA was determined using the molar absorption coefficient ($\varepsilon = 6600\ M^{-1}\ cm^{-1}$). In all experimental studies 1×10^{-3} M stock compound **1** solution was prepared by using DMSO and each batch was freshly prepared. The absorbance measurement experiments were carried out by keeping compound **1** concentration constant (80 µM) while varying the dsDNA concentration from 20 to 120 µM (r_i = [DNA]/[compound **1**] = 0.25, 0.5, 0.75, 1.00, 1.25 and 1.50).

2.6.2. Thermal denaturation assay

The denaturation profile of dsDNA solution (120 µM) has been obtained by incrementally increasing the temperature from 10 °C to 100 °C while measuring the absorbance values at 260 nm wavelength. Then into this dsDNA solution, separately compound **1** solution (30 µM) and EtBr solution (10 µM) were added to obtain the new denaturation profile of dsDNA under the same increasing temperature conditions. Tris-HCl/NaCl buffer solution was used in the denaturation studies.

2.6.3. Viscosity measurements

The viscosity measurements were conducted twice for each sample at room temperature. The viscosity data were modelled from the viscosity curves (viscosity versus shear rate) by using Herschel-Bulkley model for samples 1–3 and power-law model for samples 4–12. Herschel-Bulkley model: $\eta = \frac{\tau_0}{\dot{\gamma}} + K\dot{\gamma}^{n-1}$ where η is apparent viscosity (Pa s), τo is yield stress (Pa), K is consistency index ($Pa.s^n$), $\dot{\gamma}$ is shear rate (s^{-1}) and n is flow behavior index (-). For Herschel-Bulkley fluids $K > 0$, $0 < n < \infty$ and $\tau_o > 0$. The power-law model: $\eta = K\dot{\gamma}^{n-1}$. For shear-thinning power-law fluids, there is no τ_o ($\tau_o = 0$), $K > 0$ and $0 < n < 1$. The data is reported as $(\eta/\eta_o)^{1/3}$ versus r (r = [compound **1**]/[DNA] = 0.25–3.0), where η_o is the viscosity of dsDNA solution alone (Lerman, 1961).

2.7. Molecular docking studies

Molecular docking calculations have been performed using AutoDock Tools and AutoDock Vina software packages (Morris et al., 2009; Trott and Olson, 2010). Discovery Studio Visualizer (Biovia, 2016) has been used for the representation of the docking results and of the interactions between compound **1** and DNA. Crystal structure of DNA has been obtained from RCSB Protein Data Bank (https://www.rcsb.org/) (PDB ID: 1BNA). Prior to docking calculations, water molecules were removed, hydrogens and Gasteiger charges were added. 3D molecular structures of compound **1** has been obtained directly from the crystallographic data.

3. Results and discussion

3.1. Crystal structure and optimised molecular geometry

The compound **1** crystallizes in the triclinic space group P-1 with unit-cell parameters $a = 7.9351(4)$ Å, $b = 11.1687(6)$ Å, $c = 16.1281(9)$ Å, $\alpha = 73.713(5)°$, $\beta = 80.362(5)°$, $\gamma = 72.882(4)°$ and $Z = 4$. The chemical parameters of

compound **1**, the details of data collection and the treatment process are given in Table 1 and the comparison of the experimental and the calculated selected bond lengths, bond angles, and the torsion angles in Table 2.

There are two symmetry-independent molecules in the asymmetric unit (Fig. 3). As shown in the Fig. 3, the molecule structure of compound **1** consists of a phthalide group and a 4,6-dimethyl-2-pyrimidine amino group linked together by nitrogen atom. The phthalide group (C1—C8/O2) and (C15-C22/O4) is planar, the largest deviation from the mean plane being −0.081 Å (for C8) and −0.089 Å (for C22), respectively. The dihedral angle between the planar phthalide group and pyrimidine ring is 59.24° (for 1) and 70.0° (for 2) (Fig. 3).

The crystal packing of compound **1** is stabilized by intermolecular N—H···N and C—H···N hydrogen bonds, which generate $R_2^2(8)$ and S5 ring motifs (Etter, 1990). Intermolecular hydrogen bonds form a three-dimensional network which is enhanced by weak C—H···π interactions (Table 3, Figs. 4 and 5) There are also intermolecular C—H···O hydrogen bond interactions.

Whether the substituted groups are effective on the aromaticity of the aromatic rings or not, it can be examined by harmonic oscillator model of aromaticity (HOMA) index, given by the following equation (Kruszewski and Krygowski, 1972; Krygowski, 1993): $\mathrm{HOMA} = 1 - \left[\frac{\alpha}{n}\sum_{i=1}^{n}\left(R_i - R_{opt}\right)^2\right]$ where n is the number of bonds in the ring, α is a constant equal to 257.7 and R_{opt} is equal to 1.388 Å for C—C bonds.

Table 1 Crystal data, data collection, and refinement details of compound **1**.

Empirical formula	$C_{14}H_{13}N_3O_2$
Formula weight	255.27 g/mol
Radiation, λ	0.71073 Å
Crystal system	Triclinic
Space group	P-1
Z	4
a	7.9351(4) Å
b	11.1687(6) Å
c	16.1281(9) Å
α	73.713(5)°
β	80.362(5)°
γ	72.882(4)°
V	1305.59(13) Å^3
D_x	1.299 Mg m^{-3}
Crystal size	Prism, colorless
	0.64 × 0.55 × 0.46 mm
T_{min}, T_{max}	0.9543, 0.9682
Measured reflections	18,886
Independent reflections	6022
θ_{min}, θ_{max}	1.97°, 28.03°
Scan range	h = −9 → 10
	k = −14 → 14
	l = −20 → 20
R[$F^2 > 2\sigma(F^2)$]	0.0464
wR(F^2)	0.1434
S	1.042
w	$1/[\sigma^2(F_o{}^2) + (0.0854P)^2]$
	where $P = (F_o^2 + 2F_c^2)/3$
$\Delta\rho_{min}$, $\Delta\rho_{max}$	−0.240 e Å^{-3}, 0.278 e Å^{-3}
R_{int} value	0.0695

For purely aromatic compounds, HOMA index is equal to 1 while it is equal to 0 for non-aromatic compounds. The HOMA indexes in the range of 0.900–0.990 and 0.500–0.900 correspond to the aromatic and the non-aromatic rings, respectively (Filarowski et al., 2002, 2008). In this study, the calculated HOMA indexes for C2—C7 and C16—C21 rings are 0.941 and 0.944, respectively, indicating that the C2-C7 and C16-C21 rings are aromatic.

Average quadratic error values (R^2) have been calculated in order to show the accordance between the results found, by using experimental results and B3LYP/6-311G (d,p) method. R^2 values of compound **1** have been found as $R^2_{(\text{for bond length})} = 0.95$ (for 1) and 0.98 (for 2); $R^2_{(\text{for bond angles})} = 0.95$ (for 1) and 0.98 (for 2); $R^2_{(\text{for torsion angles})} = 0.998$ (for 1 and 2) (Fig. 6). Results show that (B3LYP/6-311G + (d, p)) method is compatible with experimental values. One of the ways to compare the experimental and theoretically obtained geometric structures as one is to overlap one another. Fig. 6 shows that the X-ray geometry and the optimized geometries in the gas phase overlap each other. While sections of phthalide and pyrimidine in (1) molecule of title compound are totally overlapped, only phthalide sections in (2) molecule are overlapped. The section of pyrimidine shows angular deviation. This deviation is supported with R^2 (0.98) value found for the bond angles of (2) molecule, and this distinction is evaluated as a result of interaction between molecules.

3.2. Frontier molecular orbitals and electronic properties

According to the molecular orbital theory, highest occupied molecular orbital (HOMO) and lowest unoccupied molecular orbitals (LUMO) can also be called as pioneer orbitals, since they have an important role in chemical reactions. The difference between HOMO and LUMO energy values can be defined as the chemical stability of the molecule. The energy difference (ΔE) calculations between HOMO and LUMO energy values were made in the gas phase (Fig. 7). While spectroscopic analysis and biological activities of compound **1** were performed in ethanol and DMSO, respectively, therefore same solvents were also used in HOMO and LUMO energies calculations of compound **1**. The lowest ΔE value between HOMO and LUMO energies is the calculated value in ethanol ($\Delta E_{(\text{gas phase})} = 6.8209$ eV; $\Delta E_{(\text{ethanol})} = 4.8875$ eV; $\Delta E_{(\text{DMSO})} = 5.0187$ eV). This energy range shows that the molecule is stable.

3.3. Global reactivity descriptors

The highest filled molecular orbital energy (E_{HOMO}) and the lowest empty molecular orbital energy (E_{LUMO}) are the basic orbitals involved in chemical reactions (Fukui, 1982). Depending on HOMO and LUMO energy values of a molecule, the electronic reactivity parameters can be determined. The conceptual aspect of the density functional method has been amply used to understand the chemical reactivity, to define a set of chemical concepts such as the electron affinity ($A = -E_{\text{LUMO}}$), ionization potential ($I = -E_{\text{HOMO}}$), chemical hardness ($\eta = \Delta E/2$), chemical softness $\sigma = 1/2\eta$), electronegativity ($\chi = (I + A)/2$), electrophilicity index ($\omega = \mu^2/2\eta$), chemical potential ($\mu = -\chi$) and nucleophilicity index ($N = 1/\omega$) which are linked to their electronic structure and

Table 2 Comparison of the selected values of experimental and calculated bond lengths, bond angles, and torsion angles of compound **1**.

	X-Ray	DFT/B3LYP with 6–311G (d,p)		
		Gas phase	in Ethanol	in DMSO
Bond lengths (Å)				
C1— O1	1.210(2)	1.200	1.207	1.209
C1—O2	1.352(2)	1.368	1.361	1.352
C1—C2	1.446(3)	1.483	1.479	1.446
C2—C7	1.380(2)	1.386	1.388	1.380
C7—C8	1.488(2)	1.510	1.508	1.488
C8—N1	1.398(2)	1.419	1.414	1.398
C8—O2	1.480(2)	1.473	1.487	1.480
C8—H8	1.03(2)	1.090	1.089	1.029
C9—N1	1.377(2)	1.377	1.378	1.377
N1—H1	0.81(2)	1.025	1.024	0.814
Bond angles (°)				
O1—C1—O2	122.12(19)	123.132	122.427	122.134
O1—C1—C2	129.09(18)	129.259	129.507	129.093
N1—C8—O2	112.88(15)	112.092	112.142	112.892
O2—C8—C7	102.71(13)	103.328	103.012	102.705
N1—C8—H8	106.2(11)	108.034	108.931	106.197
N2—C9—N1	115.46(14)	115.344	115.468	115.467
C9—N1—C8	121.96(15)	122.304	122.410	121.962
C9—N1—H1	118.5(13)	115.532	116.239	118.423
C1—O2—C8	110.27(14)	111.445	111.193	110.278
Torsion angles (°)				
O1—C1—O2—C8	173.40(18)	178.989	178.046	173.368
C1—O2—C8—N1	133.00(16)	127.267	127.448	132.992
O1—C1—C2—C3	1.8(3)	−0.169	0.522	−178.481
O2—C1—C2—C3	−178.15(18)	−179.049	−179.049	−178.148
C6—C7—C8—O2	174.55(18)	−3.221	177.684	174.562
N2—C9—N1—C8	173.44(16)	−175.199	−177.865	173.466
N3—C9—N1—C8	−5.6(3)	6.270	3.022	5.608
O2—C8—N1—C9	87.3(2)	91.673	84.605	87.249
C7—C8—N1—C9	−155.51(16)	−151.091	−158.353	−155.520
N1—C8—O2—C1	133.00(16)	127.267	127.448	132.992

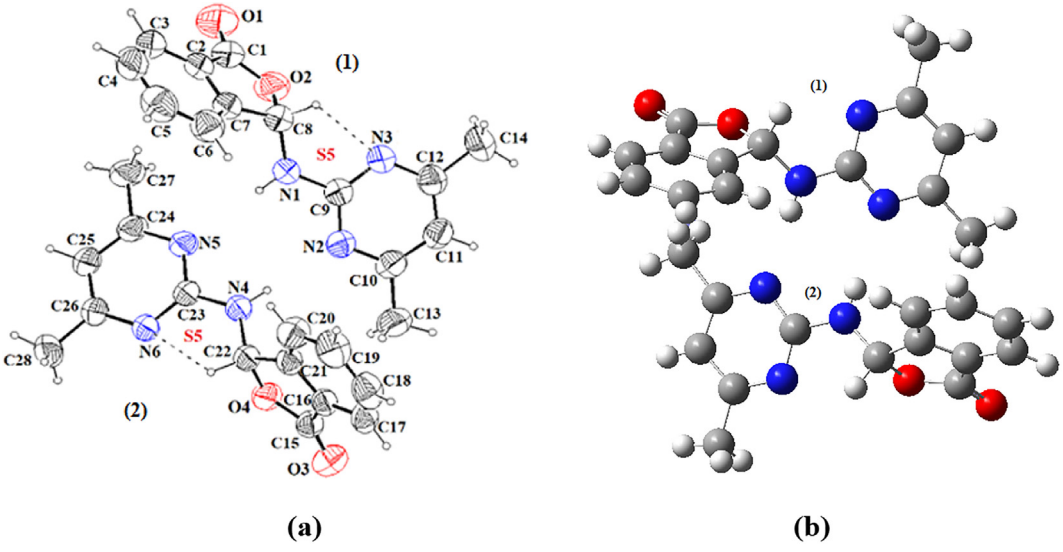

Fig. 3 An ORTEP-3 view of compound **1** with the atomic numbering scheme (a), GaussView view of the optimized molecular structure of compound **1** (b).

Table 3 Molecular interaction geometry (Å, °).

D—H···A	D—H (Å)	H···A (Å)	D—A (Å)	D—H···A (°)
N1—H1···N5^{i}	0.81	2.30	3.1115(2)	179
N4—H4A···N2^{i}	0.86	2.22	3.0747(2)	179
C5—H5···O3^{ii}	0.95	2.48	3.3958(2)	161
C8—H8···N3	1.03	2.31	2.7299(2)	103
C22—H22···N6	0.98	2.31	2.7183(2)	104
C25—H25···O3^{iii}	0.98	2.50	3.4164(2)	157
C27—H27C···O1^{iv}	0.96	2.53	3.3286(2)	141

Symmetry codes: (i) x, y, z; (ii) −1 + x, 1 + y, z; (iii) x, 1 + y, z; (iv) 1-x, 1-y, 1-z; (v) -x, -y, 1-z; (vi) 1-x, 1-y, -z

X—H	Cg	H···Cg (Å)	X—H···Cg (°)	X···Cg (Å)
C13—H13B	Cg1^{i}	2.83	141	3.6212(2)
C27—H27B	Cg2^{ii}	3.01	132	3.7164(2)
C27—H27B	Cg3^{ii}	2.84	174	3.800(2)

Symmetry codes: (i) x, y − 1, z; (ii) x, 1 + y, z; Cg1: C15/C16/C21/C22/O4; Cg2: C1/C2/C7/C8/O2; Cg3: C2/C3/C4/C5/C6/C7.

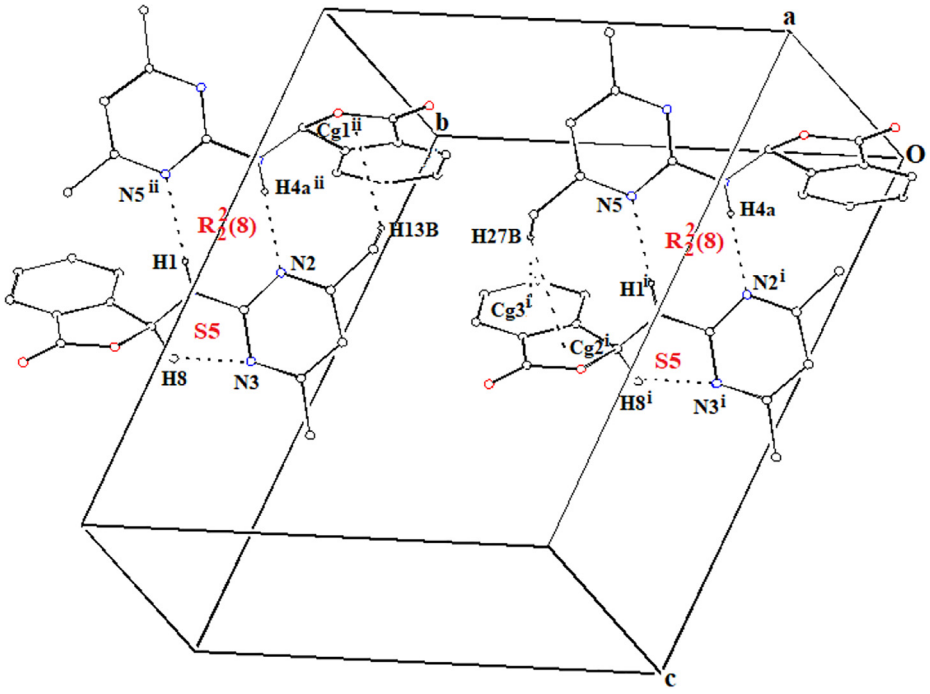

Fig. 4 A partial packing diagram for compound **1**, with N—H···N, C—H···N hydrogen bonds and C—H···π interactions shown as dashed lines [Symmetry codes: (i) x, y-1, z; (ii) x, 1 + y, z; Cg1: C15/C16/C21/C22/O4; Cg2: C1/C2/C7/C8/O2; Cg3: C2/C3/C4/C5/C6/C7].

chemical reactivity (Parr and Pearson, 1983; Pearson, 1986, 1989; Parr and Yang, 1989; Parr et al., 1999; Geerlings et al., 2003; Ghiasi and Parseh, 2014; Aboelnaga et al., 2016; Landeros-Martinez et al., 2017). The electronic reactivity parameters of compound **1** were calculated with B3LYP/6311G (d,p) method and are listed in Table 4.

The chemical hardness and softness of a molecule, calculated from the HOMO–LUMO energy gap, is a good indicator of its chemical stability. The molecules having large energy gap are known as hard and molecules having a small energy gap are known as soft molecules. A small HOMO-LUMO gap automatically means small excitation energies to the manifold of excited states. Therefore, soft molecules, with a small gap, will be more polarizable than hard molecules (Parr and Pearson, 1983; Pearson, 1986, 1989; Parr and Yang, 1989; Parr et al., 1999; Geerlings et al., 2003; Ghiasi and Parseh, 2014; Aboelnaga et al., 2016; Landeros-Martinez et al., 2017). The relatively large HOMO-LUMO energy gap indicates that compound **1** is a chemically hard molecule. Whether a given molecule is a Lewis acid or a base, it is determined by its χ value. Large χ values characterize acids and small χ values are found for bases. According to Table 4, the title compound can be defined as a Lewis acid (Parr and Pearson, 1983; Pearson, 1986, 1989; Parr and Yang, 1989; Parr et al., 1999; Geerlings et al., 2003; Ghiasi and Parseh, 2014; Aboelnaga et al., 2016; Landeros-Martinez et al., 2017).

Domingo et al. (2002) classified electrophiles based on the electrophilicity index as strong (ω > 1.50 eV), moderate

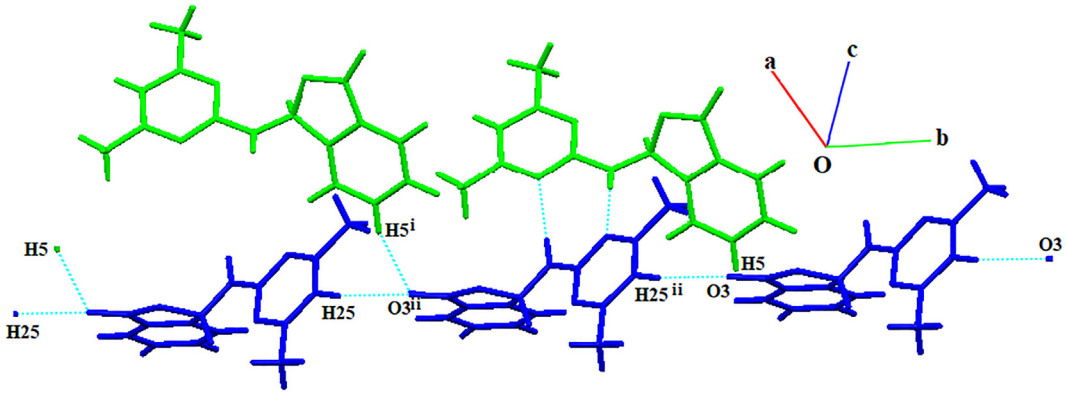

Fig. 5 Demonstration of the bonding of asymmetric units with hydrogen bonds of O3···H5 and O3···H25 for compound **1** [Symmetry codes: (i) x, y, z; (ii) −1 + x, 1 + y, z].

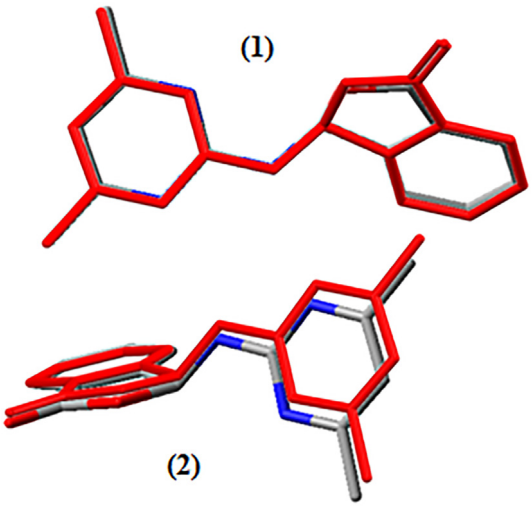

Fig. 6 Superimposition of gas phase optimized and experimental geometry (red) of compound **1**.

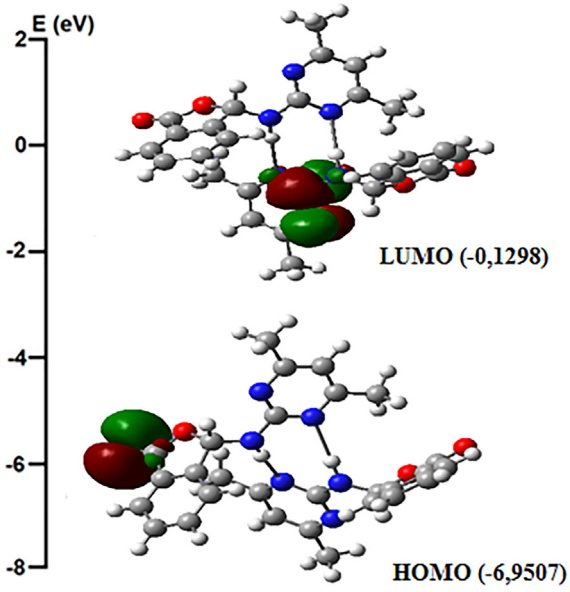

Fig. 7 The molecular orbital surfaces of compound **1** in the gas phase.

(1.50 > ω > 0.80 eV) and marginal (ω < 0.80 eV). In addition, nucleophiles are classified as strong (*N* > 3.00 eV), moderate (3.00 > *N* > 2.00 eV) and marginal (*N* < 2.00 eV) (Domingo et al., 2002; Domingo and Perez, 2013; Jaramillo et al., 2008). According to the classification, compound **1** is a strong electrophile and marginal nucleophile.

3.4. Investigation of molecular surfaces atomic charges distribution

The molecular electrostatic potential (MEP) map shows the molecular shape, size, and electrostatic potential value (Scrocco and Tomasi, 1979). The value of electrostatic potantial on MEP is determined with the system of color coding. On MEP map, while the most negative area is shown with red, the most positive area is pointed with blue color (Saraç, 2018). In this study, molecular electrostatic potential was calculated and its distributions were discussed. The 3D molecular electrostatic potential surface maps of compound **1** which is optimized by the B3LYP/6-311G (d,p) method are shown in Fig. 8. The electrostatic potential of the molecule varies in the range from $-5.888e^{-2}$ to $+5.888e^{-2}$.

Mulliken charge dispersion method is widely used to provide a broad information about the polarity of the molecule, electronic structure, dipol momentum of atomic structures, load balancing on atoms, donor and acceptor pairs providing load transfer on molecule, various features of molecular structures (Koparir et al., 2016). This method is also based on the technique of obtaining molecular orbitals with the lineer combination of atomic orbitals (Reed et al., 1985, 1988). Mulliken density analysis to calculate the atomic charges of compound **1** were calculated in Fig. 9 by calculating the B3LYP/6-311G (d, p) method. According to these results, negative charges were collected on O and N atoms with the highest electronegativity of the studied molecule. Positive charges were collected for H, whose electronegativity was lower. However, the highest positive charges were localized to the C1 and C15 (+0.405 a.u.) with C9 and C23 (+0.264 a.u.) carbons, respectively. This result indicates that the centers that are most affected by

Table 4 The frontier orbitals energies (B3LYP/6-311G (d,p)), and global reactivity parameters of compound **1**.

$E_{(HOMO)}$ (eV)	$E_{(LUMO)}$ (eV)	*DE* (eV)	I (eV)	A (eV)
−6.9507	−0.1298	6.8209	6.9507	0.1298

χ (eV)	η (eV)	σ (eV^{-1})	ω (eV)	μ (eV)	*N* (eV)
3.5403	3.4105	0.1466	1.8375	−3.5403	0.5442

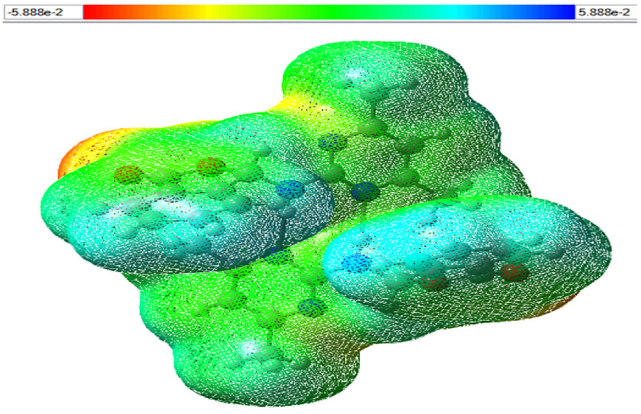

Fig. 8 Molecular electrostatic potential (MEP) of compound **1**.

nucleophiles in compound **1** are those carbon atoms. Figs. 8 and 9 clearly describe intermolecular interactions given in Table 3.

3.5. IR spectra analysis

Experimental FT-IR and theoretical IR spectra of compound **1** are shown in Fig. 10a and b, respectively. Experimental and theoretical IR spectra are computed using scale factors for comparative purposes. The assignments of the observed vibration bands have been performed and compared with the calculated frequencies. The experimental and calculated vibrational frequencies, and their assignments, are given in Table 5. It is known that DFT/B3LYP/6-311G (d,p) method calculates vibration frequencies slightly higher than their experimental values. Therefore, obtained theorotical results were rescaled by 0.9614 to approximate to experimental values (Foresman and Frisch, 1996).

The stretching vibration of C═O group of the asymmetric molecules was calculated as 1840 cm^{-1}, N─H stretching vibration was calculated as 3354 cm^{-1}, experimentally these vibrations were observed at 1753 cm^{-1} and 3240 cm^{-1}. The reason of the difference between experimental and theoretical stretching frequencies is that theorotical values are obtained in gas phase while experimental values are obtained in solid phase.

3.6. UV–Vis spectra analysis

In the recorded UV–Vis spectrum of compound **1** in ethanol, absorptions were observed at wavelengths of 205 nm, 230 nm and 280 nm. According to the method of B3LYP/6-311G (d, p), absorptions at 259 nm were observed (Fig. 11a and b). The observed values are π → π* transitions of aromatic ring

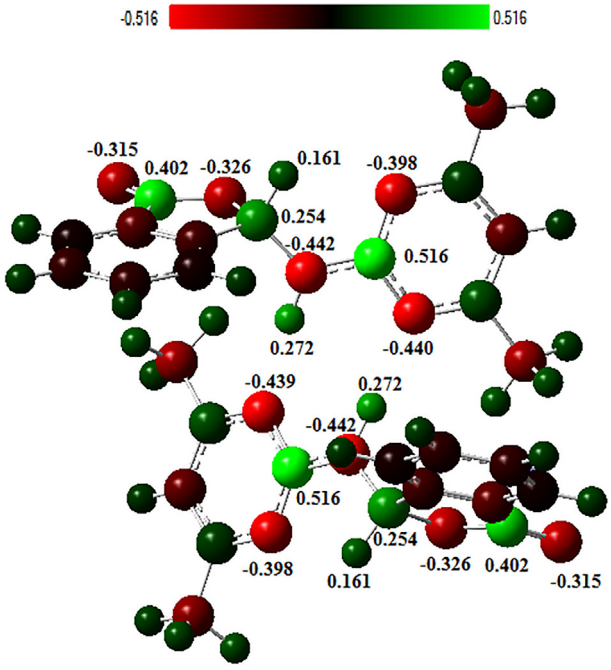

Fig. 9 Charge distribution on atoms calculated by Mulliken charge distribution method.

and the most severe experimental absorption is 230 nm while theoretical absorption is 259 nm. The experimentally observed n → π* transition at 280 nm was not clearly observed in the theoretical calculation.

3.7. NMR spectra analysis

NMR chemical deviation calculations are used to determine the structures of large molecular systems (Tamer, 2016). Therefore, in the synthesis of all organic compounds, spectrum of ^{1}H- and ^{13}C NMR are used. Moreover, usage of calculated NMR spectra along with theoretical NMR data yields more accurate results obtained. ^{1}H- and ^{13}C NMR spectra of compound **1** in DMSO d_6 are given in Figs. S1 and S2. Chemical shift values of compound **1** are calculated by using B3LYP/6-31 + G(d,p) level with GIAO method in gas state. The theoretically calculated results are compared with the experimental observations in Table 6 and Fig. 12.

3.8. Antioxidant activities

The collective studies on evaluation of the antioxidant activities of compound **1** showed that, it has minor antioxidative

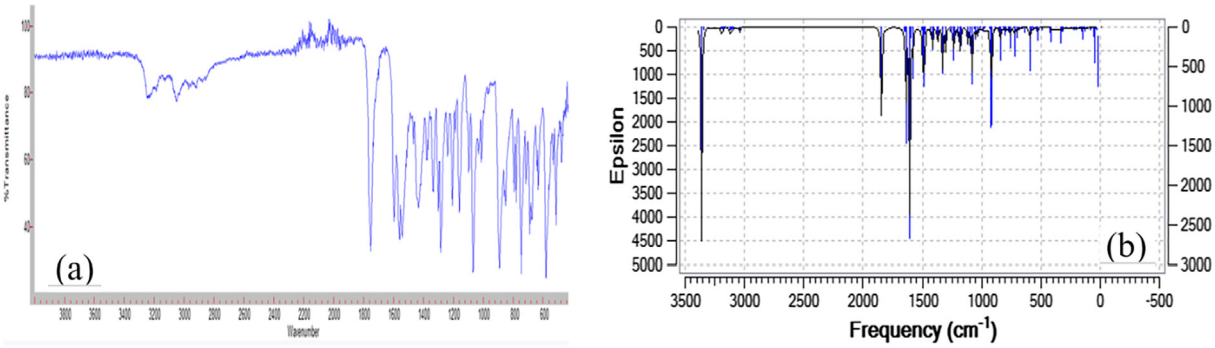

Fig. 10 FT-IR spectrum of compound **1** (a), Comparison of calculated and experimental FT-IR spectra of compound **1** (b).

ability compared to a reference substance ascorbic acid. Ascorbic acid at the same concentration with sample solution in the total phenolics content assay showed 1000 times greater activity. However; compound **1** showed slight DPPH activity in low concentration which is a method using worldwide for evaluation of the scavengering activity based on radicalic reactions. The metal chelating ability based on ferrous ions were also evaluated due to the biological and environmental importance of Fe^{2+}/Fe^{3+} ions. The compound **1** was showed considerable percentage inhibition up to 20% and in FRAP assay which is based on ferric reducing power of the compound having a reducing capability of 8.24 mM Fe(II) per g of sample. The comparative results (n = 3) of the mentioned methods are given in Table 7.

3.9. DNA binding studies

3.9.1. Absorption spectra measurements

Ultraviolet absorption spectroscopy, is one of the most preferred methods for determining nucleic acid interactions. The binding mode of the molecule being examined and changes in the structure of DNA in the presence of this molecule can

Table 5 Observed and DFT (B3LYP/6-311G (d,p)) level. Calculated vibrational frequencies of compound **1**.

Vibrational Assignments	Observed frequency (cm^{-1}) FT-IR	Calculated (B3LYP/6-311G (d,p))
>N—H, υ	3240	3354
>N—H, υ	3240	3334
=C—H, $\upsilon_{(A=C2—C7,\ B=C16—C21\ ring)}$	–	3190
=C—H, $\upsilon_{(A=C9/N2—C12,\ B=C23/N5—C26\ ring)}$	3188	3189
=C—H, $\upsilon_{(A=C2—C7,\ B=C16—C21\ ring)}$	–	3183
=C—H, $\upsilon_{(A=C2—C7,\ B=C16—C21\ ring)}$	–	3175
=C—H, $\upsilon_{(A=C2—C7,\ B=C16—C21\ ring)}$	–	3163
C—H, $\upsilon_{as(CH3)}$	3050	3132
C—H, $\upsilon_{as(CH3)}$	–	3116
C—H, $\upsilon_{(A=C8—H8,\ B=C22—H22)}$	–	3103
C—H, $\upsilon_{as(CH3)}$	–	3092
C—H, $\upsilon_{as(CH3)}$	–	3089
C—H, $\upsilon_{s(CH3)}$	–	3040
C—H, $\upsilon_{s(CH3)}$	–	3034
C=O, υ	1753	1840
C=C, $\upsilon_{(aromatic)}$	1596	1651
C=N, C=C, $\upsilon_{(aromatic)}$	1542	1604
C—H, $\delta_{(aromatic)}$; $\gamma_{(CH3)}$	–	1495
C—H, $\delta_{(A=C8—H8,\ B=C22—H22)}$	–	1376
=C—H, $\delta_{(aromatic)}$	1283	1300
C—N, υ	1205	1257
=C—H, $\delta_{(aromatic)}$	1160	1179
=C—H, $\delta_{(aromatic)}$	1098	1117
C—O, υ	1068	1077
C—O, υ	–	925
=C—H, $\gamma_{(aromatic)}$	–	887
=C—H, $\gamma_{(aromatic)}$	–	844
=C—H, $\gamma_{(aromatic)}$	–	810
=C—H, $\gamma_{(aromatic)}$	747	760
=C—H, $\gamma_{(aromatic)}$	690	753

as: Asymmetric; s: Symmetric; υ: Stretching; δ: In plane bending; γ: Out plane bending.

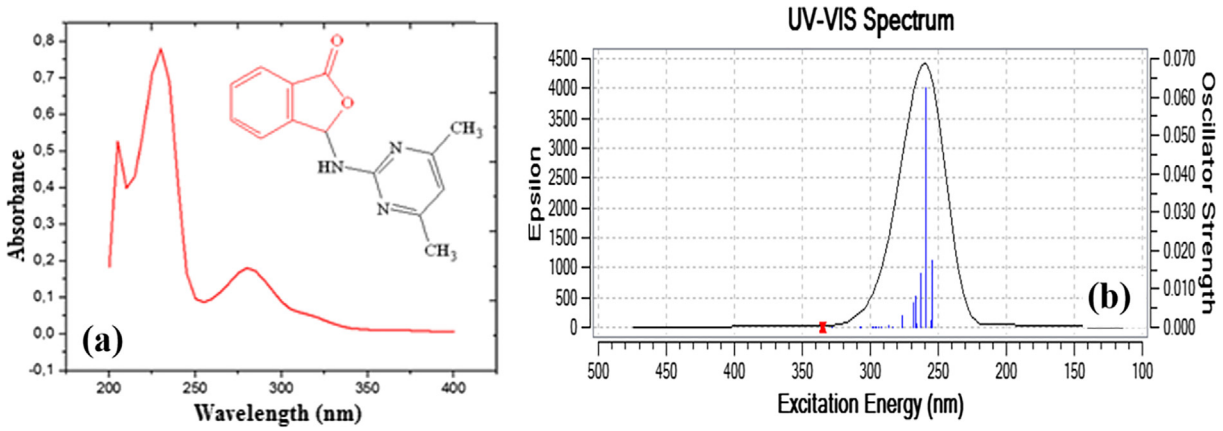

Fig. 11 UV–Vis spectrum of compound **1** (a), Comparison of calculated and experimental UV–Vis of compound **1** (b).

Table 6 Theoretically calculated (B3LYP/6-311G (d,p) level with GIAO method) and experimental ^{1}H- and ^{13}C NMR chemical shift values of compound **1,** in DMSO d_6.

Position of proton	δ_{calcd}	δ_{exp}	Position of carbon	δ_{calcd}	δ_{exp}
27-H	8.16	8.30	10-C	168.36	134.71
29-H	8.09	7.84–7.77	12-C	168.36	134.71
30-H	7.97	7.45	1-C	167.55	169.56
31-H	7.91	7.66–7-64	9-C	159.20	161.17
28-H	7.91	7.84–7.77	7-C	145.77	146.66
32-H	6.82	6.68	5-C	132.32	130.55
26-H	5.27	7.66–7-64	4-C	127.93	127.76
18-H	2.41	2.28	2-C	126.46	124.91
19-H	2.41	2.28	3-C	122.84	124.91
20-H	2.41	2.28	6-C	121.41	124.14
14-H	2.30	2.28	11-C	110.08	112.43
15-H	2.30	2.28	8-C	85.63	85.01
16-H	2.30	2.28	13-C	26.01	23.91
			17-C	26.01	23.91

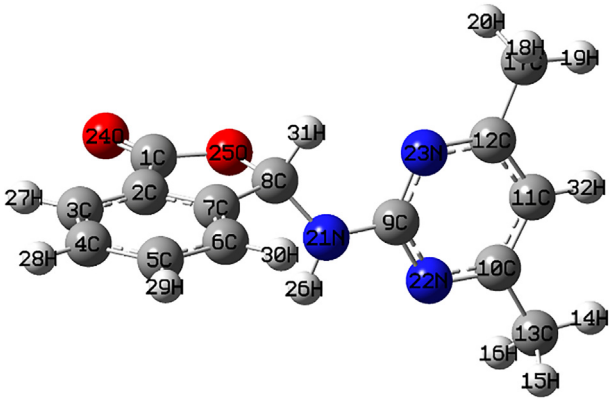

Fig. 12 Theoretically (B3LYP/6-311G (d,p)) and experimentally numbered compound **1**.

be clearly understandable from the UV–Vis spectra. The absorption of double helix DNA was caused by conjugated double bonds in the purine and pyrimidine rings within the structure. When there is an interaction between dsDNA and molecules such as compound **1**, wavelength changes in the absorption of dsDNA are observed. The interaction between DNA and such molecules varies according to the magnitude of the peak position and absorbance associated with the interaction position. In general, the absorption spectra of small molecules that bind to DNA in the groove binding mode exhibit significant hypochromic effect, while the position of the absorption band is almost unchanged; this can be explained by the fact that the electronic states of the chromophore of the complex overlap with the nitrogen groups within the grooves of DNA.

In this part of our dsDNA study, the interaction of compound **1** with dsDNA was investigated by examining the absorption spectra of the mixed solutions prepared at the specified concentrations. That is, a series of solutions were prepared by adding increasing amounts of dsDNA solution (from 10 to until reaching 200 μM) to solutions of compound **1** at a certain concentration (80 μM) in each measurement prepared from stock solutions. The UV–Vis absorption spectra of compound **1** in the absence and presence of dsDNA are given in Fig. 13. The addition of different amounts of dsDNA exhibited that the intensity of absorption decreased gradually (hypochromic effect) for about 21.50% and was not shifted in terms

Table 7 The comparative results of antioxidant activities.

Compound Name	TPs (mg GAE/mg)	FRAP (mM Fe(II)/g)	Metal Chelating	DPPH
Compound 1*	0.0034 ± 0.00	8.24 ± 0.41	20.80 ± 1.96	0.44 ± 0.01
Ascorbic Acid*	4.39 ± 0.25	–	–	84.56 ± 1.71

* 10^{-3} M.

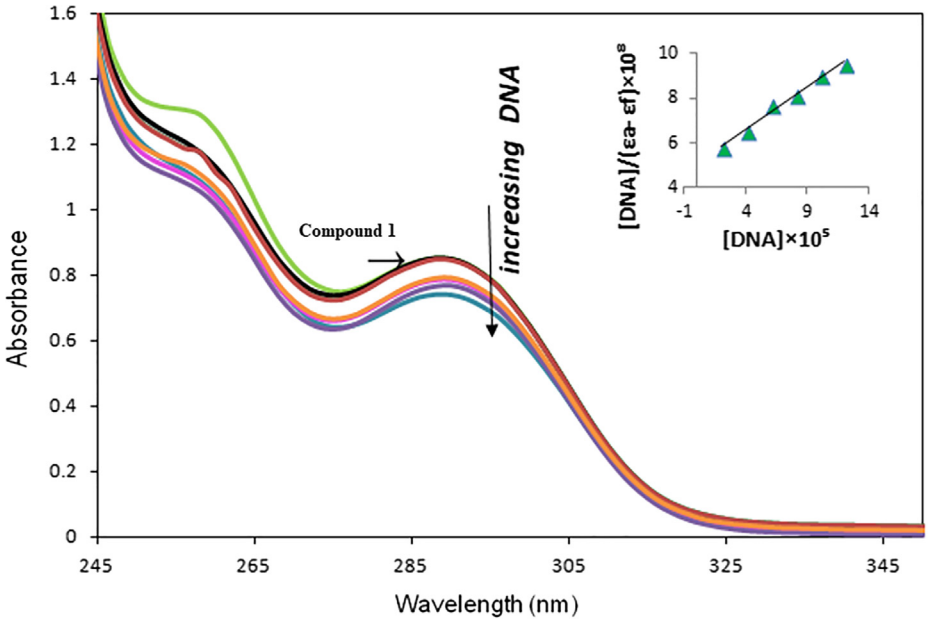

Fig. 13 UV–Vis absorption spectra of compound **1** (80 μM) upon the titration of dsDNA (20–120 μM) in Tris-HCl buffer. The arrow shows the decreases in absorbance with respect to an increase in dsDNA concentration. The maximum wavelength of compound **1** (λ_{max} = 288 nm) has not shifted. The inset shows the linear fit of [DNA]/($\varepsilon_a - \varepsilon_f$) vs. [DNA], and the binding constant (K_b) was calculated using this linearity.

of wavelength. The spectrum analysis and the changes in absorption peaks are shown in Fig. 13 clearly. The decrease in the absorbance values and the absence of significant wavelength shifts in the experiments at the constant concentrations of compound **1** showed that it was binding to dsDNA via groove binding mode. In the scientific literature, the same binding mode has been proposed in some significant drugs (Somerville et al., 2003; Shahabadi et al., 2018) with similar spectral properties, i.e., hypochromism in the presence of dsDNA and no shift in the wavelength. In addition, DNA binding constant (K_b) of compound **1** is calculated based on the titration data. The intrinsic binding constant K_b of compound **1** with dsDNA represents the binding constant per DNA base pair, can be obtained by monitoring the changes in absorbance between 200 and 400 nm with extended concentrations of dsDNA from plots [DNA]/ε_a–ε_f versus [DNA] and is given by the ratio of slope to the y-intercept, according to Benesi-Hildebrand equation (Benesi and Hildebrand, 1949): $\frac{[DNA]}{(\varepsilon_a-\varepsilon_f)} = \frac{[DNA]}{(\varepsilon_b-\varepsilon_f)} + \frac{1}{K_b\times(\varepsilon_b-\varepsilon_f)}$ where ε_a is the apparent extinction coefficient obtained by calculating A_{obsd}/[compound **1**], ε_f is the extinction coefficient of the drug-free in solution, ε_b = extinction coefficient for the drug in the fully bound form and [DNA] is the concentration of DNA in terms of base-pairs. The K_b value was $8.13 \times 10^4 \pm 0.07$ L mol^{-1} for compound **1** (from Fig. 13 and log K_b = 4.91 ± 0.04) and is lower than the known value for basic intercalator such as ethidium bromide (10^7 L mol^{-1}). However, this K_b value is highly consistent with the previously reported K_b value (9.59×10^4), as the minor groove binding phthalide ligand which is investigated in our previous report (Yılmaz et al., 2020). It has been found that compound **1** was bounded to dsDNA by the groove binding mode, but more experimental methods are needed to confirm the binding mechanism more precisely, so that the thermal denaturation, viscosity measurements, and theoretical studies are good tools to obtain information about the binding mode (see Scheme 1).

3.9.2. Thermal denaturation studies

The stability of the secondary structure of dsDNA resulting from the binding of compound **1** to the dsDNA strand is often widely determined by the thermal denaturation technique. The melting temperature of the dsDNA is an important consideration showing the interaction of small molecules with nucleic acids. As the temperature of the dsDNA solution medium increases, the hydrogen bonds between the base pairs in the dsDNA structure break and the dsDNA structure begins to

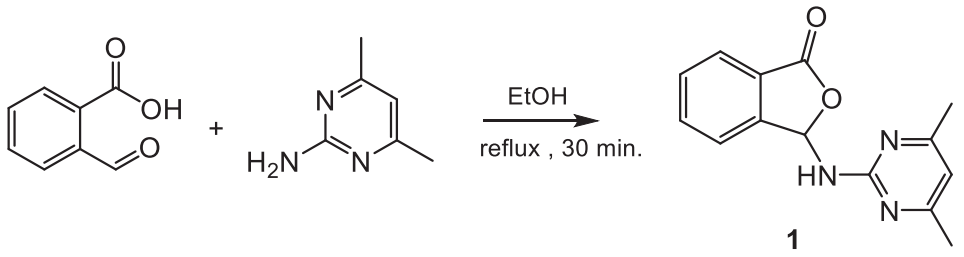

Scheme 1 Synthesis of 3-((4,6-dimethylpyrimidin-2-yl)amino)isobenzofuran-1(3*H*)-one (**1**).

decompose into single strands. The temperature at which half of the total base pairs separate is defined as the melting temperature (T_m) of DNA (Marmur and Doty, 1962). T_m is an extremely important parameter for the balance of the double helical structure. The molecules change their T_m values depending on their binding affinity to DNA. As can be seen from Fig. 14, the denaturation process for compound **1** is completed in one step. In the absence of compound **1**, the T_m value of 120 μM dsDNA was measured as 72.2 °C. Also, as shown in Fig. 14, the T_m value of dsDNA solution was not significantly increased by the addition of compound **1** (at a given concentration). As an example, at $r = 0.083$, the T_m value of dsDNA was 77.8 °C and the temperature difference was 5.6 °C, a pretty low increase in DNA melting temperature, suggesting that the introducing of this compound doesn't diminish the stability of DNA's double helical conformation. The T_m value of EtBr compound + dsDNA solution was much greater (83.4 °C, temperature difference: 11.2 °C in Fig. 14) compared to compound **1**'s introduction into DNA indicating that EtBr interacted by intercalation (as known) with dsDNA, but compound **1** was not bound to dsDNA by intercalation. This is clear evidence that compound **1** was not bounded to the dsDNA construct by intercalation (Arya et al., 2003).

3.9.3. Viscosity measurements

The consistency indices for viscosity studies, the flow behavior indices and the calculated apparent viscosities at 20 s^{-1} of samples were given in Table 8 at the shear rate of 20 s^{-1}. Samples 1–3 in Table 8 fit the Herschel-Bulkley model. However, samples 4–12 showed pseudoplastic behavior since $0 < n < 1$ and no flow event was observed. As can be seen from Table 8, the yield stress values of samples 1–3 were almost the same. The consistency index values of Example 1 (Tris-HCl/NaCl buffer solution) were lower compared to example 2 (dsDNA solution) and 3 (compound **1** solution), but the flow behavior index values had an inverse tendency. The apparent viscosity values of samples 2 and 3 are higher than the apparent viscosity of sample 1. It is evident that the apparent viscosities of examples 4–12 (dsDNA + compound **1**) are increased compared to the apparent viscosity values of examples 1–3. According to these data, the effect of increasing amount of compound **1** on the relative viscosity of dsDNA has been given in Fig. 15. As noted in the literature, there is often no change in viscosity since electrostatic or groove surface binders tend to be very small (Arya et al., 2003). However, the increase in viscosity of the nucleic acid solution is a clear indication that the binding mode is intercalation (Mirzaei-Kalar, 2018).

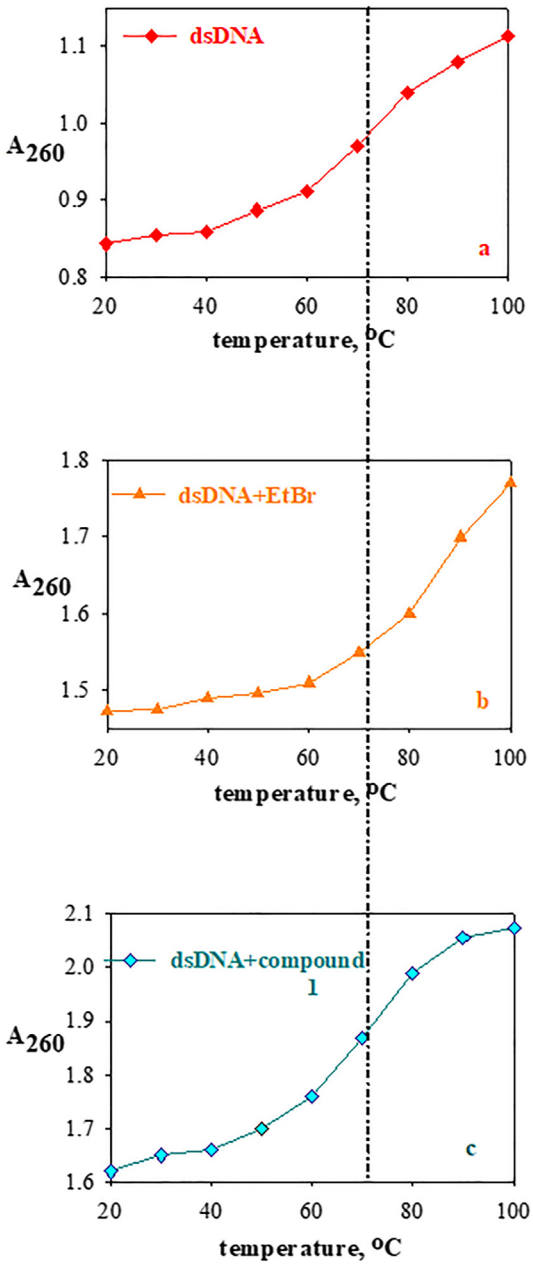

Fig. 14 The thermal denaturation profiles of dsDNA (120 μM) (a) in the absence and in the presence of EtBr (10 μM) (b) and compound **1** (30 μM) (c) in Tris-HCl/NaCl buffer solution.

Table 8 The Herschel-Bulkey parameters and calculated apparent viscosities at 20 s^{-1}.

Sample no	Yield stress (Pa)	K ($Pa.s^n$)	n (-)	Apparent viscosity (mPa.s) at 20 s^{-1}
Buffer	0.30 ± 0.02	$1.10 \times 10^{-4} \pm 2.32 \times 10^{-4}$	1.46 ± 0.02	15.43
Compound **1**	0.30 ± 0.03	$2.68 \times 10^{-4} \pm 1.00 \times 10^{-4}$	1.28 ± 0.01	15.62
dsDNA	0.31 ± 0.01	$8.92 \times 10^{-5} \pm 2.22 \times 10^{-5}$	1.50 ± 0.05	15.90
Sample 1	0.32 ± 0.01	$1.85 \times 10^{-4} \pm 1.85 \times 10^{-5}$	1.40 ± 0.03	16.61
Sample 2	0.31 ± 0.01	$3.62 \times 10^{-4} \pm 1.54 \times 10^{-4}$	1.32 ± 0.01	16.44
Sample 3	0.32 ± 0.02	$1.37 \times 10^{-4} \pm 2.00 \times 10^{-4}$	1.45 ± 0.04	16.53
Sample 4	0.30 ± 0.02	$3.41 \times 10^{-4} \pm 1.98 \times 10^{-4}$	1.30 ± 0.02	15.84
Sample 5	0.33 ± 0.00	$4.54 \times 10^{-4} \pm 2.31 \times 10^{-4}$	1.30 ± 0.03	17.62
Sample 6	0.33 ± 0.00	$4.18 \times 10^{-4} \pm 3.87 \times 10^{-4}$	1.32 ± 0.01	17.60
Sample 7	0.33 ± 0.04	$4.78 \times 10^{-4} \pm 1.01 \times 10^{-4}$	1.28 ± 0.01	17.60
Sample 8	0.32 ± 0.02	$8.61 \times 10^{-4} \pm 7.41 \times 10^{-4}$	1.23 ± 0.01	17.71
Sample 9	0.32 ± 0.01	$1.52 \times 10^{-3} \pm 4.70 \times 10^{-5}$	0.83 ± 0.04	16.91
Sample 10	0.34 ± 0.04	$6.10 \times 10^{-4} \pm 1.98 \times 10^{-4}$	0.66 ± 0.05	17.22
Sample 11	0.33 ± 0.01	$1.44 \times 10^{-4} \pm 2.33 \times 10^{-4}$	1.11 ± 0.06	16.70
Sample 12	0.33 ± 0.01	$3.21 \times 10^{-4} \pm 5.63 \times 10^{-4}$	1.15 ± 0.03	17.00

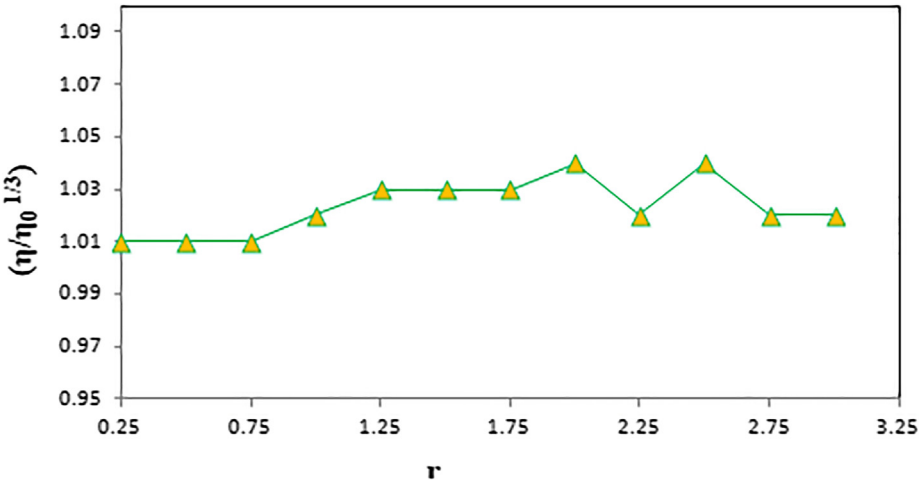

Fig. 15 Effect of increasing amount of compound **1** on the relative viscosity of dsDNA.

3.10. Molecular docking studies

Molecular docking calculations have been performed for compound **1** to determine the docking poses and to reveal the possible interactions between the investigated compound **1** and DNA. It has been observed that the compound **1** takes place mainly in the minor groove of DNA. Additionally, some non-bonded molecular interactions have also been observed between the compound **1** and the consecutive base pairs of DNA. It can be said that this compound **1** – base pair interactions may cause an elongation and/or an unwinding in DNA structure and thus a partial intercalation. In Fig. 16, binding modes and compound **1** – DNA interactions compound **1** are represented. The characteristics of the interactions are given in Table 9. It was observed that hydrogen bonds take part in the stabilization of compound **1** – DNA complex, in addition to hydrogen bonds, Pi – alkyl interactions also contribute to the stabilization of the compound **1** – DNA complex. The binding affinities of the lowest energy docking poses was found to be −8.3 kcal/mol for compound **1**.

4. Conclusions

A novel 3-substituted phthalide derivative (compound **1**) was synthesized and characterized by various spectral techniques. The single-crystal X-ray analysis shows that compound **1** crystallizes in the triclinic space group P-1 with unit-cell parameters a = 7.9351(4) Å, b = 11.1687(6) Å, c = 16.1281(9) Å, α = 73.713(5)°, β = 80.362(5)°, γ = 72.882(4)° and Z = 4. A complete vibrational analysis and geometry optimization of the related compound were carried out at the DFT level by using the hybrid functional B3LYP with 6-311G(d,p) basis set. DNA binding studies of compound **1** were investigated by UV–Vis, thermal denaturation and viscosity measurements. In the mentioned techniques, the mode of binding of compound **1** to dsDNA is determined as a minor groove with a binding constant of $8.13 \times 10^4 \pm 0.07$ L mol^{-1}. In molecular docking studies, it was observed also the investigated compound takes place in the minor groove of DNA. It was also observed that compound interacts with the consecutive base pairs of DNA. It was thought that these interactions may cause elongation and/or unwinding in DNA structure and thus partial intercalation. On the other hand, investigated compound shows satisfactorily high binding affinity with the value −8.3 kcal/mol. The title compound was screened also for its antioxidant activity by

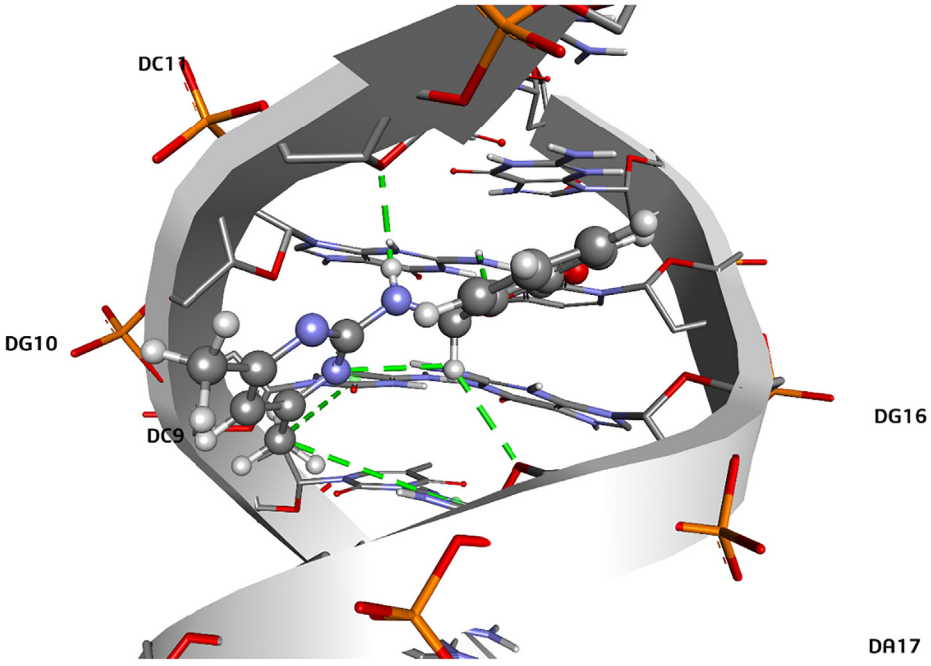

Fig. 16 Binding mode and compound – DNA interactions for compound **1**.

Table 9 Interactions between DNA and compound **1**.

Interaction No	DNA Strand	Nucleotide	Nucleotide Atom	Compound 1 Atom	Distance (Å)	Nature of Interaction
1	A	DC11	O4′	H1	2.32	Conventional H-Bond
2	A	DG10	H21	O2	2.17	Conventional H-Bond
3	B	DG16	H21	N2	2.96	Conventional H-Bond
4	B	DA17	O4′	H6	2.61	Carbon H-Bond
5	A	DC9	Ring	C13	5.41	Pi – Alkyl
6	B	DA17	Ring	C13	5.21	Pi – Alkyl

DPPH, FRAP and TP assays. Further efforts on the development of other analogs derivatives are currently underway in our laboratory. We hope that newly synthesized 3-substituted phthalide derivative will provide an opportunity for synthesis of new heterocyclic compounds that may have considerable applications in initial phases of drug development.

Declaration of Competing Interest

The authors declare that they have no known competing financial interests or personal relationships that could have appeared to influence the work reported in this paper.

Acknowledgments

The authors wish to thank Istanbul Technical University, Faculty of Science and Letters, Department of Chemistry for some experimental conditions, and Dr. Filiz ALTAY (Istanbul Technical University, Department of Food Engineering, Faculty of Chemical and Metallurgical Engineering) for viscosity measurements and her valuable comments.

Appendix A. Supplementary material

Supplementary data to this article can be found online at https://doi.org/10.1016/j.arabjc.2020.03.013.

References

Aboelnaga, A., Hagar, M., Soliman, S.M., 2016. Ultrasonic synthesis, molecular structure and mechanistic study of 1,3-dipolar cycloaddition reaction of 1-alkynylpyridinium-3-olate and acetylene derivatives. Molecules 21, 848–861.

Arora, P., Arora, V., Lamba, H.S., Wadhwa, D., 2012. Importance of heterocyclic chemistry: a review. Int. J. Pharm. Sci. Res. 3, 2947–2954.

Arya, D.P., Micovic, L., Charles, I., Coffee, R.L., Willis, B., Xue, L., 2003. Neomycin binding to Watson-Hoogsteen (W-H) DNA triplex groove: a model. J. Am. Chem. Soc. 125, 3733–3744.

Bauernschmitt, R., Ahlrichs, R., 1996. Treatment of electronic excitations within the adiabatic approximation of time dependent density functional theory. Chem. Phys. Lett. 256, 454–464.

Beck, J.J., Chou, S.-C., 2007. The structural diversity of phthalides from the Apiaceae. J. Nat. Prod. 70, 891–900.

Benesi, H.A., Hildebrand, J.H., 1949. A spectrophotometric investigation of the interaction of iodine with aromatic hydrocarbons. J. Am. Chem. Soc. 71, 2703–2707.

Benzie, I.F., Strain, J.J., 1996. The ferric reducing ability of plasma (FRAP) as a measure of "Antioxidant Power": The FRAP assay. Anal. Biochem. 239, 70–76.

Beyazit, N., Kaya, K., Şenel, P., Özdemir, A.D., Gölcü, A., 2019. Crystal structure and DNA binding properties of khellin oxime. J. Molec. Str. 1197, 450–457.

Biovia, D.S., 2016. Discovery studio visualizer, v17.2.0.16349, Dassault Systèmes, San Diego.

Blois, M.S., 1958. Antioxidant determinations by the use of a stable free radical. Nature 181, 1199–1200.

Casida, M.E., Jamorski, C., Casida, K.C., Salahub, D.R., 1998. Molecular excitation energies to high-lying bound states from time-dependent density-functional response theory: characterization and correction of the time-dependent local density approximation ionization threshold. J. Chem. Phys. 108, 4439–4449.

Dennington, R., Keith, T., Millam, J., 2009. GaussView, Version 5. Semichem Inc., Shawnee Mission KS.

Dinis, T.C., Madeira, V.M., Almeida, L.M., 1994. Action of phenolic derivates (acetoaminophen, salycilate and 5-aminosalycilate) as inhibitors of membrane lipid peroxidation and as peroxyl radical scavengers. Arch. Biochem. Biophys. 315, 161–169.

Domingo, L.R., Aurell, M.J., Perez, P., Contreras, R., 2002. Quantitative characterization of the global electrophilicity power of common diene/dienophile pairs in Diels-Alder reactions. Tetrahedron 58, 4417–4423.

Domingo, L.R., Perez, P., 2013. Global and local reactivity indices for electrophilic/nucleophilic free radicals. Org. Biomol. Chem. 11, 4350–4358.

Du, J., Yu, Y., Ke, Y., Wang, C., Zhua, L., Qian, Z.M., 2007. Ligustilide attenuates pain behavior induced by acetic acid or formalin. J. Ethnopharmacol. 112, 211–214.

Dua, R., Shrivastava, S., Sonwane, S.K., Srivastava, S.K., 2011. Pharmacological significance of synthetic heterocycles scaffold: a review. Adv. Biol. Res. 5, 120–144.

Everaere, K., Scheffler, J.-L., Mortreux, A., Carpentier, J.-F., 2001. Stereoselective synthesis of 3-substituted phtalides via asymmetric transfer hydrogenation using well-defined ruthenium catalysts under neutral conditions. Tetr. Lett. 42, 1899–1901.

Etter, M.C., 1990. Encoding and decoding hydrogen-bond patterns of organic compounds. Acc. Chem. Res. 23, 120–126.

Farrugia, L.J., 1999. *WinGX* suite for small-molecule single-crystal crystallography. J. Appl. Cryst. 32, 837–838.

Farrugia, L.J., 1997. ORTEP-3 for Windows - a version of ORTEP-III with a Graphical User Interface (GUI). J. Appl. Cryst. 30. 565–565.

Filarowski, A., Koll, A., Glowiak, T., 2002. Low barrier hydrogen bonds in sterically modified Schiff bases. J. Chem. Soc. Perkin Trans. 2, 835–842.

Filarowski, A., Kochel, A., Kluba, M., Kamounah, F.S., 2008. Structural and aromatic aspects of tautomeric equilibrium in hydroxy aryl Schiff bases. J. Phys. Org. Chem. 21, 939–944.

Foresman, J.B., Frisch, A.E., 1996. Exploring Chemistry with Electronic Structure Methods. Gaussian Inc., Pittsburg, PA.

Frisch, M.J., Trucks, G.W., Schlegel, H.B., Scuseria, G.E., Robb, M. A., Cheeseman, J.R., Scalmani, G., Barone, V., Mennucci, B., Petersson, G.A., Nakatsuji, H., Caricato, M., Li, X., Hratchian, H. P., Izmaylov, A.F., Bloino, J., Zheng, G., Sonnenberg, J.L., Hada, M., Ehara, M., Toyota, K., Fukuda, R., Hasegawa, J., Ishida, M., Nakajima, T., Honda, Y., Kitao, O., Nakai, H., Vreven, T., Montgomery, J.A., Peralta, J.E., Ogliaro, F., Bearpark, M., Heyd, J.J., Brothers, E., Kudin, K.N., Staroverov, V.N., Keith, T., Kobayashi, R., Normand, J., Raghavachari, K., Rendell, A., Burant, J.C., Iyengar, S.S., Tomasi, J., Cossi, M., Rega, N., Millam, J.M., Klene, M., Knox, J.E., Cross, J.B., Bakken, V., Adamo, C., Jaramillo, J., Gomperts, R., Stratmann, R.E., Yazyev, O., Austin, A.J., Cammi, R., Pomelli, C., Ochterski, J.W., Martin, R.L., Morokuma, K., Zakrzewski, V.G., Voth, G.A., Salvador, P., Dannenberg, J.J., Dapprich, S., Daniels, A.D., Farkas, O., Foresman, J.B., Ortiz, J.V., Cioslowski, J., Fox, D.J., 2010. Gaussian 09. Gaussian Inc, Wallingford CT.

Fukui, K., 1982. Role of frontier molecular orbitals in chemical reactions. Science 218, 747–754.

Geerlings, P., Proft, F.D., Langenaeker, W., 2003. Conceptual density functional theory. Chem. Rev. 103, 1793–1874.

Gelat, F., Lebrun, S., Henry, N., Agbossou-Niedercorn, F., Michon, C., Deniau, E., 2017. Total synthesis of (–)-herbaric acid through organocatalyzed asymmetric halolactonization of acrylate-type benzoic acids. Synlett. 28, 225–230.

Ghiasi, R., Parseh, N., 2014. Quantum mechanical study of the structure, NBO and HOMO–LUMO analysis of molecule Ooxaliplatinium. J. Appl. Chem. Res. 8, 25–33.

Gubiani, J.R., Teles, H.L., Silva, G.H., Young, M.C.M., Pereira, J.O., Bolzanin, V.S., Araujo, A.R., 2017. Cyclo-(trp-phe) diketopiperazines from the endophytic fungus Aspergillus versicolor isolated from Piper aduncum. Quim. Nova 40, 138–142.

Harper, J.K., Arif, A.M., Ford, E.J., Strobel, G.A., Porco Jr., J.A., Tomer, D.P., Oneill, K.L., Heider, E.M., Grant, D.M., 2003. Pestacin: a 1,3-dihydro isobenzofuran from *Pestalotiopsis microspora* possessing antioxidant and antimycotic activities. Tetr. 59, 2471–2476.

Ibrahim, G.I., Jalal, A.F., Ibrahim, B.M., 2013. Evaluation of antioxidant activity, phenolic, flavonoid and ascorbic acid contents of three edible plants from Erbil/Kurdistan. Tikrit J. Pure Sci. 18, 46–51.

Jaramillo, P., Domingo, L.R., Chamorro, E., Perez, P., 2008. A further exploration of a nucleophilicity index based on the gas-phase ionization potentials. J. Mol. Struct. Theochem. 865, 68–72.

Karmakar, R., Pahari, P., Mal, D., 2014. Phthalides and phthalans: synthetic methodologies and their applications in the total synthesis. Chem. Rev. 114, 6213–6284.

Koparir, P., Sarac, K., Orek, C., Koparir, M., 2016. Molecular structure, spectroscopic properties and quantum chemical calculations of 8-t-buthyl-4-methyl-2H-chromen-2-one. J. Mol. Struct. 1123, 407–415.

Krishnan, R., Binkley, J.S., Seeger, R., Pople, J.A., 1980. Selfconsistent molecular orbital methods. XX. A basis set for correlated wave functions. J. Chem. Phys. 72, 650–654.

Kruszewski, J., Krygowski, T.M., 1972. Definition of aromaticity basing on the harmonic oscillator model. Tetr. Lett. 13, 3839–3842.

Krygowski, T.M., 1993. Crystallographic studies of inter- and intramolecular interactions reflected in aromatic character of.pi.-electron systems. J. Chem. Inf. Comput. Sci. 33, 70–78.

Lamberth, C., Dinges, J. (Eds.), 2012. Bioactive heterocyclic compound classes: Pharmaceuticals. Wiley-VCH Verlag&Co, Weinheim, Germany.

León, A., Del-Ángel, M., Ávila, J.L., Delgado, G., 2017. Phthalides: distribution in nature, chemical reactivity, synthesis, and biological activity. Prog. Chem. Org. Nat. Prod. 104, 127–246.

Lerman, L.S., 1961. Structural considerations in the interaction of DNA and acridines. J. Mol. Biol. 3, 18–30.

Liu, C.-L., Liao, S.-J., Zeng, J.-S., Lin, J.-W., Li, C.-X., Xie, L.-C., Shi, X.-G., Huang, R.-X., 2007. dl-3n-butylphthalide prevents stroke via improvement of cerebralmicrovessels in RHRSP. J. Neurol. Sci. 260, 106–113.

Landeros-Martinez, L.-L., Glossman-Mitnik, D., Orrantia-Borunda, E., Flores, N., 2017. Theoretical calculation of UV-Vis, IR spectra and reactivity properties of Tamoxifen drug: A methodology comparison. MOJ Biorg. Org. Chem. 1, 87–96.

Ma, F., Gao, Y., Qiao, H., Hu, X., Chang, J., 2012. Antiplatelet activity of 3-butyl-6-bromo-1(3H)-isobenzofuranoneon rat platelet aggregation. J. Thromb. Thrombolysis 33, 64–73.

Macrae, C.F., Edgington, P.R., McCabe, P., Pidcock, E., Shields, G. P., Taylor, R., Towler, M., Van de Streek, J., 2006. Mercury:

Visualization and analysis of crystal structures. J. Appl. Crystallogr. 39, 453–457.
Marmur, J., Doty, P., 1962. Determination of the base composition of deoxyribonucleic acid from its thermal denaturation temperature. J. Molec. Biol. 5, 109–118.
Mirzaei-Kalar, Z., 2018. In vitro binding interaction of atorvastatin with calf thymus DNA: multispectroscopic, gel electrophoresis and molecular docking studies. J. Pharm. Biomed. Anal. 161, 101–109.
Morris, G.M., Huey, R., Lindstrom, W., Sanner, M.F., Belew, R.K., Goodsell, D.S., Olson, A.J., 2009. AutoDock4 and AutoDockTools4: automated docking with selective receptor flexibility. J. Comput. Chem. 30, 2785–2791.
Odabasoglu, M., Büyükgüngör, O., 2006. 3-(4-Hydroxyanilino)isobenzofuran-1(3*H*)-one. Acta Cryst. 62, 1879–1881.
Oliveira, R.J., Navarro, S.D., de Lima, D.P., Meza, A., Pesarini, J.R., Gomes, R.S., Karaziack, C.B., Mauro, M.O., Cunha-Laura, A.L., Monreal, A.C.D., Romao, W., Junior, V.L., Beatriz, A., 2015. A novel cytosporone 3-Heptyl-4,6-dihydroxy-3H-isobenzofuran-1-one: synthesis; toxicological, apoptotic and immunomodulatory properties; and potentiation of mutagenic damage. BMC Cancer 15, 1–15. Article Number: 561.
Pahari, P., Senapati, B., Mal, D., 2004. Regiospecific synthesis of isopestacin, a naturally occurring isobenzofuranone antioxidant. Tetr. Lett. 45, 5109–5112.
Palillero-Cisneros, A., Bedolla-Medrano, M., Ordóñez, M., 2018. Efficient $PhB(OH)_2$-catalyzed one-pot synthesis of 3-substituted isoindolin-1-ones and isobenzofuran-1(3*H*)-ones under solvent free conditions. Tetr. 74, 4174–4181.
Parr, R.G., Pearson, R.G., 1983. Absolute hardness: companion parameter to absolute electronegativity. J. Am. Chem. Soc. 105, 7512–7516.
Parr, R.G., Yang, W., 1989. Density Functional Theory of Atoms and Molecules. Oxford University Press, Oxford, New York.
Parr, R.G., Szentpaly, L., Liu, S., 1999. Electrophilicity Index. J. Am. Chem. Soc. 121, 1922–1924.
Pearson, R.G., 1986. Absolute electronegativity and hardness correlated with molecular orbital theory. Proc. Nati. Acad. Sci. USA 83, 8440–8441.
Pearson, R.G., 1989. Absolute electronegativity and hardness: applications to organic chemistry. J. Org. Chem. 54, 1423–1430.
Prlainović, N.Ž., Rančić, M.P., Stojiljković, I., Nikolić, J.B., Drmanić, S.Ž., Ajaj, I., Marinković, A.D., 2018. Experimental and theoretical study on solvent and substituent effects on the intramolecular charge transfer in 3-[(4-substituted)phenylamino] isobenzofuran-1(3*H*)-ones. J. Serb. Chem. Soc. 83, 139–155.
Quin, L.D., Tyrell, J.A., 2010. Fundamentals of Heterocyclic Chemistry: Importance in Nature and in the Synthesis of Pharmaceuticals. John Wiley & Sons Inc, Hoboken, NewJersey.
Reed, A.E., Weinstock, R.B., Weinhold, F., 1985. Natural population analysis. J. Chem. Phys., 735–746
Reed, A.E., Curtiss, L.A., Weinhold, F., 1988. Intermolecular interactions from a natural bond orbital, donor-acceptor viewpoint. Chem. Rev. 88, 899–926.
Runge, E., Gross, E.K.U., 1984. Density-functional theory for time-dependent systems. Phys. Rev. Lett. 52, 997–1000.
Saraç, K., 2018. Synthesis and theoretical chemical calculations of 4-chloromethyl-6,8-dimethylcoumarin compound. BEU Journal of Science 7, 311–319.
Sellal, A., Belattar, R., Bouzidi, A., 2019. Heavy metals chelating ability and antioxidant activity of Phragmites Australis stems extracts. J. Ecol. Eng. 20, 116–123.
Scrocco, E., Tomasi, J., 1979. Electronic molecular structure, reactivity and intermolecular forces: an euristic interpretation by means of electrostatic molecular potentials. Adv. Quant. Chem. 11, 115–193.
Shahabadi, N., Shiri, F., Hadidi, S., 2018. The effect of dimerization on the interaction of ibuprofen drug with calf thymus DNA: molecular modeling and spectroscopic investigation. Nucleosides, Nucleotides Nucl. Acids 37, 147–168.
Sheldrick, G.M., 1997. SHELXS-97 and SHELXL-97, Program for the solution and refinement of crystal structures. University of Gottingen, Germany.
Sheldrick, G.M., 2015. Crystal structure refinement with SHELXL. Acta Cryst. C71, 3–8.
Singleton, V.L., Rossi, J.A., 1965. Colorimetry of total phenolics with phosphomolybdic-phosphotungstic acid reagents. Amer. J. Enol. Viticult. 16, 144–158.
Somerville, L., Krynetski, E.Y., Krynetskaia, N.F., Beger, R.D., Zhang, W., Marhefka, C.A., Evans, W.E., Kriwacki, R.W., 2003. Structure and dynamics of thioguanine-modified duplex DNA. J. Biol. Chem. 278, 1005–1011.
Stephens, P.J., Devlin, F.J., Chabalowski, C.F., Frisch, M.J., 1994. Ab Initio calculation of vibrational absorption and circular dichroism spectra using density functional force fields. J. Phys. Chem. 98, 11623–11627.
Stierle, A.A., Stierle, D.B., Girtsman, T., 2012. Caspase-1 inhibitors from an extrennophilic fungus that target specific leukemia cell lines. J. Nat. Prod. 75, 344–350.
Stratmann, R.E., Scuseria, G.E., Frisch, M.J., 1998. An efficient implementation of time-dependent density-functional theory for the calculation of excitation energies of large molecules. J. Chem. Phys. 109, 8218–8224.
Strobel, G., Ford, E., Worapong, J., Harper, J.K., Arif, A.M., Grant, D.M., Fung, P.C.W., Chau, R.M.W., 2002. Isopestacin, an isobenzofuranone from *Pestalotiopsis microspora*, possessing anti-fungal and antioxidant activities. Phytochem. 60, 179–183.
Şenel, P., Agar, S., Sayin, V.O., Altay, F., Yurtsever, M., Gölcü, A., 2020. Elucidation of binding interactions and mechanism of Fludarabine with dsDNA via multispectroscopic and molecular docking studies. J. Pharm. Biomed. Anal. 179, 112994.
Tamer, Ö., 2016. Structural, spectroscopic, electronic and nonlinear optical investigations on cis-2,6-bis(2-chlorophenyl)-3,3-dimethylpiperidin-4-one. SAU Fen Bil. Der. 20, 565–571.
Teixeira, R.R., Bressan, G.C., Pereira, W.L., Ferreira, J.G., Oliveira F. M. Thomaz, D.C., 2013. Synthesis and antiproliferative activity of C-3 functionalized isobenzofuran-1(3H)-ones. Molecules 18, 1881–1896.
Trott, O., Olson, A.J., 2010. AutoDock Vina: Improving the speed and accuracy of docking with a new scoring function, efficient optimization, and multithreading. J. Comput. Chem. 31, 455–461.
Yılmaz, Z.T., Odabaşoğlu, H.Y., Şenel, P., Adımcılar, V., Erdoğan, T., Özdemir, A.D., Gölcü, A., Odabaşoğlu, M., 2020. A novel 3-((5-methylpyridin-2-yl)amino)isobenzofuran-1(3*H*)-one: molecular structure describe, X-ray diffractions and DFT calculations, antioxidant activity, DNA binding and molecular docking studies. J. Molec. Str. 1205, 127585.
Zhang, H., Zhang, S., Liu, L., Luo, G., Duan, W., Wang, W., 2010. Synthesis of chiral 3-substituted phthalides by a sequential organocatalytic enantioselective aldol-lactonization reaction. Three-step synthesis of (S)-(−)-3-Butylphthalide. J. Org. Chem. 75, 368–374.